Aligned Growth of Millimeter-Size Hexagonal Boron Nitride Single-Crystal Domains on Epitaxial Nickel Thin Film

Junhua Meng, Xingwang Zhang, Ye Wang, Zhigang Yin, Heng Liu, Jing Xia, Haolin Wang, Jingbi You, Peng Jin, Denggui Wang, and Xiang-Min Meng*

Atomically thin hexagonal boron nitride (h-BN) is gaining significant attention for many applications such as a dielectric layer or substrate for graphene-based devices. For these applications, synthesis of high-quality and large-area h-BN layers with few defects is strongly desirable. In this work, the aligned growth of millimeter-size single-crystal h-BN domains on epitaxial Ni (111)/sapphire substrates by ion beam sputtering deposition is demonstrated. Under the optimized growth conditions, single-crystal h-BN domains up to 0.6 mm in edge length are obtained, the largest reported to date. The formation of large-size h-BN domains results mainly from the reduced Ni-grain boundaries and the improved crystallinity of Ni film. Furthermore, the h-BN domains show well-aligned orientation and excellent dielectric properties. In addition, the sapphire substrates can be repeatedly used with almost no limit. This work provides an effective approach for synthesizing large-scale high-quality h-BN layers for electronic applications.

1. Introduction

Hexagonal boron nitride (h-BN) has attracted considerable research interest in recent years due to its unique properties such as wide band gap, high thermal conductivity, low dielectric constant, chemical inertness, and high mechanical strength.[1–4] Ultrasmooth surface and low density of dangling bonds/trapped charges make atomically thin h-BN a promising candidate as dielectric or substrate layers for other 2D materials.[5–11] Indeed, the electron mobility values of graphene on h-BN were drastically increased compared to the commonly used SiO_2/Si substrate,[5] and the device performance was improved when h-BN was used as a dielectric layer.[7–11] For electronic applications, synthesis of high-quality and large-area h-BN layers with few defects is strongly desirable.

Generally, large-size domains lead to a low density of domain boundary defects, resulting in a higher quality of film, while the limited domain size and unavoidable domain boundaries in h-BN films always significantly impair the performance of electronic devices.[12,13] To obtain as large single-crystal h-BN domains as possible, a common strategy is to suppress nucleation density during the growth process. In earlier reports, the sizes of h-BN domains were limited to several micrometers.[2,14–17] Thus far, numerous efforts have been devoted to synthesize large-size h-BN domains on various transition metals by optimizing the growth parameters or pretreating the substrate surface.[18–23] Recently, single-crystal h-BN domains with lateral dimensions

J. H. Meng, Prof. X. W. Zhang, Y. Wang, Dr. Z. G. Yin, H. Liu, Dr. H. L. Wang, Prof. J. B. You, Prof. P. Jin, D. G. Wang
Key Lab of Semiconductor Materials Science
Institute of Semiconductors
Chinese Academy of Sciences
Beijing 100083, P. R. China
E-mail: xwzhang@semi.ac.cn

J. H. Meng, Prof. X. W. Zhang, Y. Wang, Dr. Z. G. Yin, H. Liu, Dr. H. L. Wang, Prof. J. B. You, Prof. P. Jin, D. G. Wang
College of Materials Science and Opto-Electronic Technology
University of Chinese Academy of Sciences
Beijing 100049, P. R. China

Dr. J. Xia, Prof. X.-M. Meng
Key Lab of Photochemical Conversion and Optoelectronic Materials
Technical Institute of Physics and Chemistry
Chinese Academy of Sciences
Beijing 100190, P. R. China

DOI: 10.1002/smll.201604179

© 2017 Wiley-VCH Verlag GmbH & Co. KGaA, Weinheim

exceeding 100 μm have been demonstrated using Cu–Ni alloy[13] and $Fe/SiO_2/Si$[24] as substrates by chemical vapor deposition (CVD) technique. Our previous studies have also revealed that the 110 μm single-crystal h-BN domains can be obtained on Ni foils by ion beam sputtering deposition (IBSD).[25] Nevertheless, further enlarging h-BN domain size remains a challenge. Moreover, the prolific nucleation and growth of misoriented domains on polycrystalline metal surfaces lead to the formation of domain boundary defects by coalescence. An effective approach for reducing or even eliminating domain boundaries is growing aligned h-BN domains and stitching them together to form a uniform h-BN layer. Actually, it has been reported that aligned monolayer h-BN domains were epitaxially grown on single-crystal substrates like Ru (0001), Ir (111), and Ni (111) in ultrahigh vacuum (UHV) system.[26–29] However, the UHV process requires expensive and sophisticated equipment, and these studies were only focused on the electronic and surface properties by various in situ characterization techniques. Moreover, the growth of aligned h-BN domains on facilely transferred Ge and Cu substrates was also demonstrated,[22,23,30,31] whereas the h-BN domain size was only a few micrometers. Obviously, achieving large-size h-BN domains with the same orientation is an effective way to improve quality of h-BN layers.

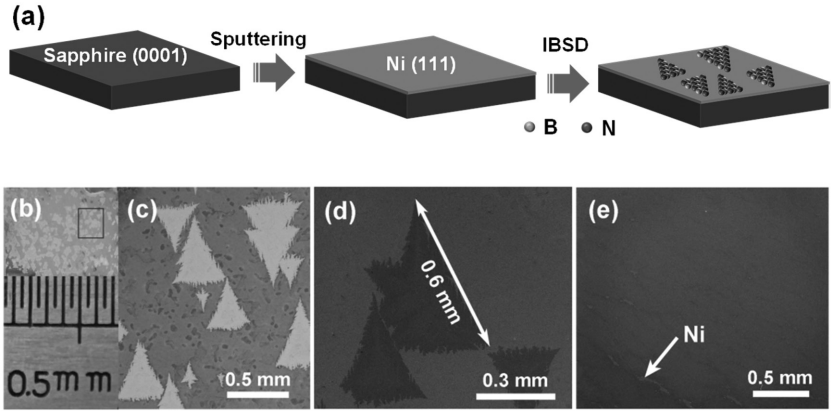

Figure 1. Millimeter-size h-BN domains on epitaxial Ni (111)/sapphire substrates. a) Schematic of the growth process of h-BN layers on the epitaxial Ni (111)/sapphire substrates. b) Photograph of the h-BN/Ni surface with oxidation treatment in air. c) Enlarged optical microscopy image of the marked area in (b). d) SEM image of individual h-BN domains achieved under the optimized growth conditions. e) SEM image of a continuous and uniform h-BN layer deposited with prolonged growth time. The white arrow indicates the occasionally observed bare Ni substrate.

In this work, we report the synthesis of millimeter-size single-crystal h-BN domains by IBSD on the Ni (111) films, which were epitaxially grown on sapphire (0001) substrates. It is found that the single-crystal Ni film with a smooth surface and less grain boundary is a critical factor for growing large-size h-BN domains. Under the optimized growth conditions, the single-crystal h-BN domains up to 0.6 mm in edge length were obtained. Due to the close lattice match between h-BN and Ni (111), these h-BN domains exhibit well-aligned orientation. The merged h-BN layer exhibits quite uniform and excellent dielectric behavior. Furthermore, the h-BN on a repeatedly used sapphire substrate has almost the same quality as that obtained originally. This work provides an effective approach for synthesizing large-scale high-quality h-BN layers for electronic applications.

2. Results and Discussion

The growth of h-BN on the epitaxial Ni films was carried out in an IBSD system, and the growth process is schematically illustrated in **Figure 1**a. First, the cleaned *c*-plane sapphire substrates were loaded into a magnetron sputtering chamber for the deposition of Ni films at 600 °C in pure Ar atmosphere. The crystalline quality of epitaxial Ni films on sapphire substrates is excellent as revealed by the X-ray diffraction (XRD) and transmission electron microscopy (TEM) measurements, and the epitaxial relationship between Ni and sapphire is determined to be $Ni(111)[11\bar{2}]//sapphire(0001)[11\bar{2}0]$ (Figure S1, Supporting Information). It is worth to note that for a perfect single-crystal Ni (111), a threefold symmetry should be expected in the Φ scan. Herein, the observed sixfold symmetry arises from the two sets of Ni crystallites in different sequences of atom layers (*ABC* or *ACB*) with an azimuthal orientation 60° apart.[32] The close intensities of two sets of XRD peaks in the Φ scan suggest that the two twin orientations are almost equally distributed. After that, the h-BN was grown on the epitaxial Ni (111) films by IBSD and the details are described in the Experimental Section.

Our previous studies indicated that ion beam density and growth temperature play a critical role in the h-BN domain size, and both the higher temperature and the lower density of ion beam lead to a larger size of h-BN domains.[25] In this work, the optimum conditions were determined to be the growth temperature of 1050 °C and the ion beam density of 0.1 mA cm^{-2} (Figures S2 and S3, Supporting Information). Following the IBSD process, the h-BN/Ni was heated in air at 500 °C for 15 min and the oxidation of unprotected Ni surface makes the h-BN domains optically visible, as shown in Figure 1b. The enlarged optical microscope image of the marked area in Figure 1b is presented in Figure 1c, where millimeter-size h-BN domains can be clearly identified. Figure 1d shows the scanning electron microscopy (SEM) image of individual h-BN domains achieved under the optimized growth conditions. The largest length of side for the h-BN domains reaches 0.6 mm, which is five times larger than those in previous reports (the improvement of the area by a factor of about 20).[13,25] The statistic plot of the domain size distribution yielded an average h-BN size of about 0.4 mm (Figure S4, Supporting Information). Most of the h-BN domains shown in the SEM and optical microscopy images have a well-defined triangular shape, implying the single-crystal nature of h-BN domains. The edges of some domains are sawtoothed, which is attributed to diffusion instabilities, as reported previously.[24,25,33] Furthermore, the triangular h-BN domains in Figure 1c,d exhibit only two

 © 2017 Wiley-VCH Verlag GmbH & Co. KGaA, Weinheim

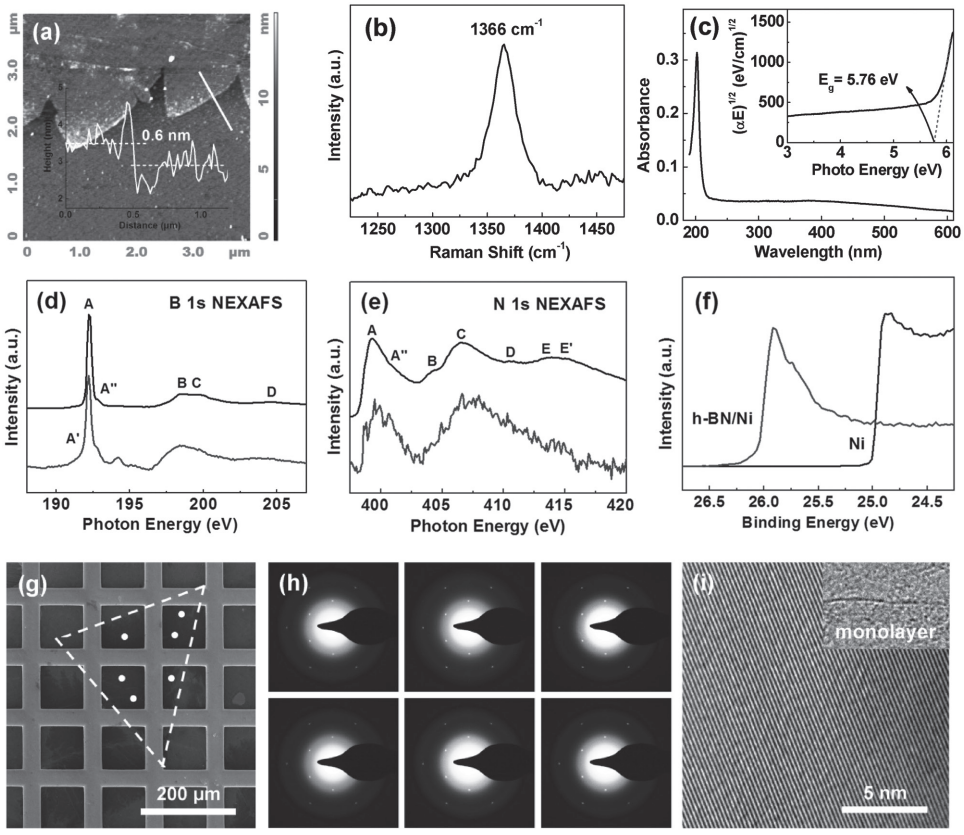

Figure 2. Characterization of h-BN domains. a) AFM image of h-BN domains transferred onto a 300 nm SiO_2/Si substrate. The inset presents the height profile along the white line drawn in (a). b) Raman spectrum of h-BN domains on a SiO_2/Si substrate. c) UV–vis spectrum of h-BN layer transferred on a transparent quartz substrate. The inset shows optical band gap (5.76 eV) analysis of h-BN from (c). d,e) Normalized B 1s and N 1s NEXAFS of bulk h-BN (reference thick film, upper curves) and h-BN domain (lower curves). f) UPS spectra around the secondary-electron threshold region for the h-BN/Ni and Ni substrate. g) Low-magnification SEM image of an h-BN domain on a carbon-covered TEM grid. h) SAED patterns recorded at different locations labeled in (g). The six diffraction patterns obtained from well-spaced regions of the domain have identical orientation, thus confirming it is a single crystal. i) Top-view HRTEM image of h-BN domains. The inset shows a folded edge, reconfirming the monolayer nature of the h-BN domain.

opposite orientations, suggesting that they are aligned along the lattice of the Ni (111) surface (this will be discussed later). With prolonged growth time, the well-aligned h-BN domains were in contact with the adjacent ones and merged into a continuous layer, forming a uniform h-BN layer over the entire region (Figure 1e). Except for occasionally observed bare Ni substrates, as indicated by the white arrow in Figure 1e, the merged h-BN layer shows uniform color contrast.

Figure 2a shows the atomic force microscopy (AFM) image of the h-BN domains transferred onto a SiO_2/Si substrate, the thickness of the h-BN domain is estimated to be about 0.6 nm from the step height profile at the domain edge (the inset of Figure 2a), consistent with the monolayer h-BN. Figure 2b shows a typical Raman spectrum of the transferred h-BN layer on a SiO_2/Si substrate with a characteristic peak at about 1366 cm^{-1}, arising from the E_{2g} vibrational mode of h-BN,[34] and a narrow full width at half maximum (FWHM) of 22 cm^{-1}. X-ray photoelectron spectroscopy (XPS) measurements reveal that the B 1s and N 1s core-level peaks are located at 190.3 and 398.2 eV (Figure S5, Supporting Information), respectively, consistent with the previously reported values for the h-BN on Ni.[13,16,25,35–37] Figure 2c shows the UV–vis absorption spectrum of the h-BN layer transferred onto a quartz substrate, and a strong absorption peak is observed at ≈200 nm, characteristics of 2D h-BN. By using the formula for an indirect band semiconductor,[38,39] the optical band gap of h-BN is estimated to be 5.76 eV (the inset of Figure 2c), which is slightly smaller than the previously reported values.[15,39,40]

Near-edge X-ray absorption fine structure (NEXAFS) was applied to characterize the electronic structures of the h-BN domains on Ni surface, as shown in Figure 2d,e. The observed spectral features are similar to the reported results of the monolayer h-BN chemisorbed on Ni (111).[35] All spectral features for both B 1s and N 1s NEXAFS of the h-BN can be divided into two groups: features labeled A, A′, and A″ reflect transitions of a core electron into the states of π symmetry, while all the remaining features correspond to transitions with predominantly in-plane σ character.[35,36] Besides, the significant difference in NEXAFS spectra between the h-BN domains and the bulk h-BN (reference thick film) implies the 2D features of the obtained h-BN. In addition, based on the ultraviolet photoelectron spectroscopy (UPS) spectra (Figure 2f), the work functions of Ni and h-BN/Ni are determined to be 5.00 and 3.93 eV, respectively. The work function drops by 1.07 eV, which is lower than that of

 © 2017 Wiley-VCH Verlag GmbH & Co. KGaA, Weinheim

the chemisorbed h-BN on Ni (111) (1.7–1.8 eV),[29,35,41] suggesting the weaker coupling to the Ni substrate in this work.

Figure 2g shows a low-magnification SEM image of the large-size h-BN domains after they were transferred onto a carbon-covered TEM grid, where a triangular h-BN domain is well preserved and its edges are outlined by the white dashed lines. Selected area electron diffraction (SAED) patterns (Figure 2h) were recorded at six different locations, marked by the white dots in the SEM image. Apparently, all the SAED patterns show one set of sixfold symmetric diffraction spots with identical orientation, confirming the single-crystal nature of the large-size h-BN domain.[18,24,25] A top-view high-resolution TEM (HRTEM) image (Figure 2i) shows the characteristic h-BN lattice constant of 0.25 nm, and the cross-sectional TEM image taken at the folded domain edge (the inset of Figure 2i) reconfirms the monolayer nature of the h-BN domain. We proposed that two mechanisms, surface-mediated reaction and gas phase nucleation/growth, are responsible for the growth of h-BN on Ni substrates, depending on the flux of BN species.[25] Under the lower flux of BN species (the ion beam densities ranging from 0.1 to 0.4 mA cm^{-2}), the gas phase nucleation can be ignored due to the much lower concentration of precursors. Therefore, after a full monolayer is formed, the growth rate of h-BN significantly drops, leading to predominately monolayer h-BN. When the ion beam density increased to 0.7 mA cm^{-2} (i.e., the higher flux of BN species), both the surface-mediated reaction and the gas phase nucleation occur, resulting in mostly bilayer h-BN sheets, as revealed by the SEM and TEM images (Figure S6, Supporting Information).

To evaluate the dielectric properties of h-BN layers, the electron tunneling through the h-BN layer was investigated by using conductive AFM (CAFM) measurements. As shown in **Figure 3**a, the active h-BN layer is sandwiched between the Ni substrate and a Pt-coated AFM probe. Figure 3b shows the current–voltage (I–V) curves taken from the Ni surface and the h-BN layers with different thicknesses under the same conditions, respectively. In contrast to an Ohmic behavior of Ni surface, the I–V curves of h-BN layers show a linear behavior at low bias due to direct tunneling, and an exponential rise in current at high bias implying the onset of dielectric breakdown in the h-BN layers, which is in good agreement with the results of exfoliated h-BN.[42] The CAFM image of h-BN layer on Ni (the inset of Figure 3b) exhibits a uniform distribution of tunneling current with a distinct boundary, signaling different thicknesses of barrier. Figure 3c shows comparison of the tunneling conductance extracted from the low bias linear regime of h-BN layers on Ni (111) with that of exfoliated h-BN.[42] Based on Figure 3c, the thicknesses of h-BN layers are estimated to be 0.42 and 1.39 nm, respectively, corresponding to a monolayer and four-layer h-BN. Combining with the thickness and the dielectric breakdown voltage obtained using the constant current method (the voltage at which the current reaches 0.1 nA), the dielectric breakdown strength of h-BN is estimated to be 7.15 MV cm^{-1}, which is close to that of exfoliated h-BN.[42] In the high bias region, the tunneling process is dominated by field-emission tunneling across the barrier and the tunneling current becomes nonlinear. The high bias data of the

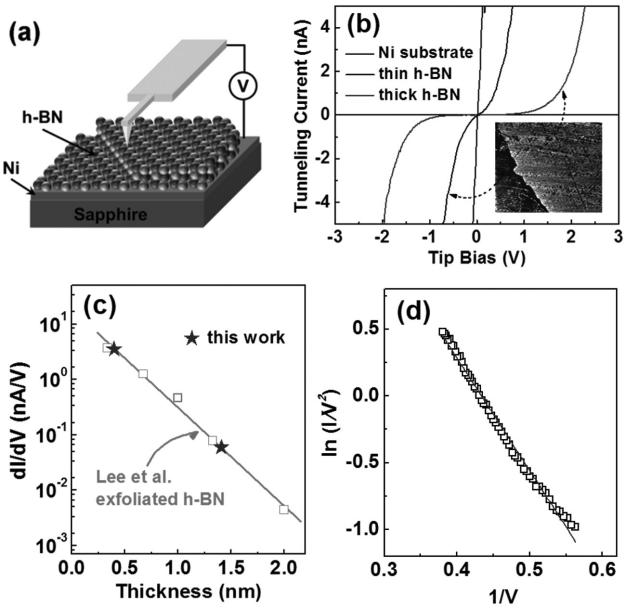

Figure 3. Electron tunneling through monolayer and few-layer h-BN. a) Schematic of measurement setup in CAFM. b) I–V curves of the h-BN layer with different thicknesses and the Ni substrate. Inset shows tunneling current image of the h-BN layer on Ni. c) Comparison of the tunneling conductance extracted from the linear region (low bias) of h-BN layer on Ni (111) grown by IBSD with that of exfoliated h-BN.[42] d) $\ln(I/V^2)$ versus $1/V$ curve in a high bias region for fitting of Fowler–Nordheim tunneling model.

four-layer h-BN were fitted by using the Fowler–Nordheim (FN) tunneling model, and the $\ln(I/V^2)$ versus $1/V$ curve in the high bias region is shown in Figure 3d. A clear linear dependence in this plot confirms that the tunneling through h-BN at high bias can be explained by FN model. These results demonstrate uniform and excellent dielectric behavior and the absence of charged impurities and defects of the h-BN.

Surface morphology of substrate is one of the most important factors to limit the nucleation density (and thus the size of h-BN domains). In the following experiments, in order to obtain the single-crystal Ni (111) film with a smooth surface for growing large-size h-BN domains, we systematically investigated the growth of Ni films by magnetron sputtering. The Ni films were deposited on sapphire (0001) substrates at 600 °C. The thicknesses of Ni films varied from 0.3 to 2.5 µm by varying the deposition time, as determined by cross-sectional SEM observations (Figure S7, Supporting Information). The as-grown Ni films are composed of interconnected Ni grains and the size of Ni grains increases with increasing thickness, as shown in Figure S8 (Supporting Information). To improve their crystalline quality, the as-grown Ni films were annealed in vacuum at 1050 °C for 20 min. **Figure 4**a–d shows the bright field polarized optical microscopy images of the annealed Ni films, in which grain boundaries (appeared as grooves or protrusions) are more visible and easily distinguished. For all the annealed Ni films, the size of Ni grains is an order of magnitude larger than that of the as-grown films. More importantly, with the increase of Ni thickness, the size of Ni grains increases, and the density of grain boundaries significantly decreases. The similar phenomena are also

 © 2017 Wiley-VCH Verlag GmbH & Co. KGaA, Weinheim

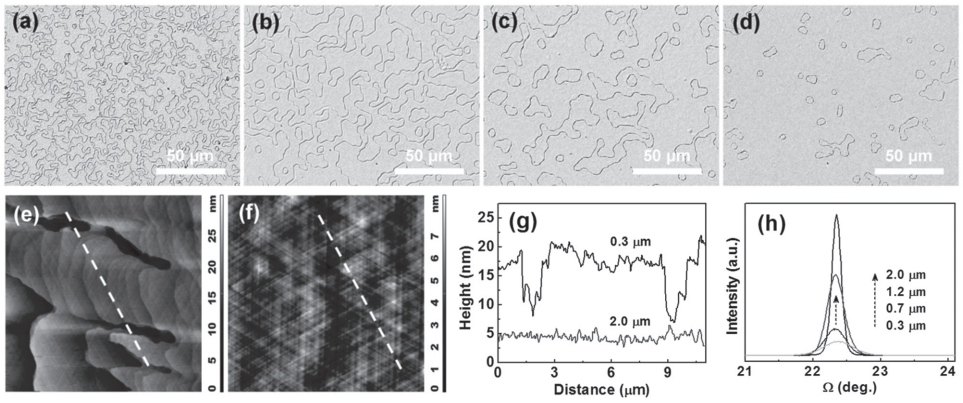

Figure 4. Characterization of epitaxial Ni (111) films. Bright field polarized optical microscopy images of the annealed Ni films with different thicknesses of a) 0.3, b) 0.7, c) 1.2, and d) 2.0 μm. AFM images of the annealed e) 0.3 and f) 2.0 μm Ni films (scan area is 10×10 μm^2). g) The height profile along the white lines drawn in (e) and (f), indicating a significant difference in roughness between two Ni films. h) Rocking curves of the Ni (111) reflection for the annealed Ni films with various thicknesses.

demonstrated by the corresponding SEM images (Figure S9, Supporting Information). The surface morphology of the 0.3 and 2.0 μm Ni films was further characterized by AFM, as shown in Figure 4e,f. For the 0.3 μm Ni film, the height undulation along the white dotted line is ≈15 nm (Figure 4g). In contrast, a rather flat surface without any grain boundaries was observed within the scanned area for the 2.0 μm Ni film, and the height undulation is only ≈2.0 nm, which is an order of magnitude lower than that of the 0.3 μm film. To judge the epitaxial quality of these Ni films, the rocking curves of the Ni (111) reflection were recorded, as shown in Figure 4h. As the thickness of Ni films is increased, the rocking curve becomes sharper suggesting an improved crystallinity, which is consistent with the above optical microscopy images. The FWHM of the Ni (111) rocking curve is as narrow as 0.160° for the 2.0 μm film, revealing a perfect crystallinity.

Figure 5a–d shows the SEM images of h-BN domains synthesized on the Ni films with the thickness of 0.3, 0.7, 1.2, and 2.0 μm at a fixed growth temperature of 1050 °C and an ion beam density of 0.1 mA cm^{-2} for 15 min, respectively. Noticeably, the thicker Ni films result in a significant decrease in the nucleation density, and thus the size of h-BN domains dramatically increases. From previous reports on the influence of substrate surface morphology on the growth of h-BN, it is known that the rough surfaces or presence of grain boundaries are likely to act as nucleation seeds, leading to an enhanced rate of nucleation.[18,19,25] We propose that the improved surface morphology (especially the reduced Ni-grain boundary) with increasing Ni thickness plays a key role in the increasing size of h-BN domains. In this work, grooves or protrusions are formed at the Ni-grain boundaries, as demonstrated in Figure 4, leading to an increased roughness of Ni surface. A reduced surface diffusivity and a lower effective surface energy for rough surfaces, which diminishes Gibbs free energy barrier, facilitate heterogeneous nucleation.[19] As a result, the higher density of grain boundaries will lead to the enhanced rate of nucleation and thus the smaller size of h-BN domain. To quantitatively evaluate the effects of Ni-grain boundary on the h-BN growth, the lengths of Ni-grain boundaries were extracted from Figure 4a–d by ImageJ software (Figure S10, Supporting Information). For comparison, these lengths were normalized in terms of the corresponding value for the 2.0 μm film. Figure 5e shows both the maximum lateral size and the density of h-BN domains as a function of the normalized length of Ni-grain boundaries. The size of h-BN domains increases from 70 μm to 0.56 mm with the density of domains decreasing from 95 to 6 mm^{-2}, when the normalized length of Ni-grain boundaries reduces by one order of magnitude (from 10.2 to 1.0) with increasing Ni film thickness from 0.3 to 2.0 μm. As the thickness of Ni film further increases to 2.5 μm, however, the size of h-BN domains has no obvious change, which is attributed to the similar morphology of the 2.0 and 2.5 μm Ni films (Figure S11, Supporting Information). These results suggest that the smooth surface is crucial to suppress the nucleation of h-BN, and the formation of large-size h-BN domains is mainly due to the reduced grain boundaries and the improved crystallinity of underlying Ni films. It will be expected to achieve the more large-size h-BN domains on an atomic smooth single-crystal Ni (111) surface.

It can also be seen from Figure 5a–d that all the triangular h-BN domains have two orientations that are rotated by 60° from each other, which is equivalent to 180° mirror symmetry resulting from the different polarities of B–N bonds.[31] Of all the areas we have inspected, both orientations are almost equally distributed, indicating that there is little or no preference to one particular h-BN orientation on the Ni (111) surface. It has also been reported that two antiparallel h-BN domains can coexist even on a single-crystal Ni (111) substrate.[43,44] Since the lattice mismatch between h-BN monolayer and Ni (111) is about –0.4%, a commensurate 1×1 structure for h-BN/Ni (111) is expected. Previous calculations suggested that the triangular h-BN domains are expected to have all N-terminated zigzag edges due to the lower edge energy,[45] and N atoms preferentially sit on top of Ni atoms because of the strong hybridization of N lone pairs with Ni atoms.[46] Accordingly, two different orientations of h-BN domains with respect to the underlying Ni (111) substrate can be proposed, as shown in Figure 5f. N atoms sit on top of every outermost Ni atoms, while B atoms either on fcc (N, B) = (top, fcc) or hcp (N, B) = (top, hcp) hollow sites, respectively. Density functional calculations indicated that

 © 2017 Wiley-VCH Verlag GmbH & Co. KGaA, Weinheim

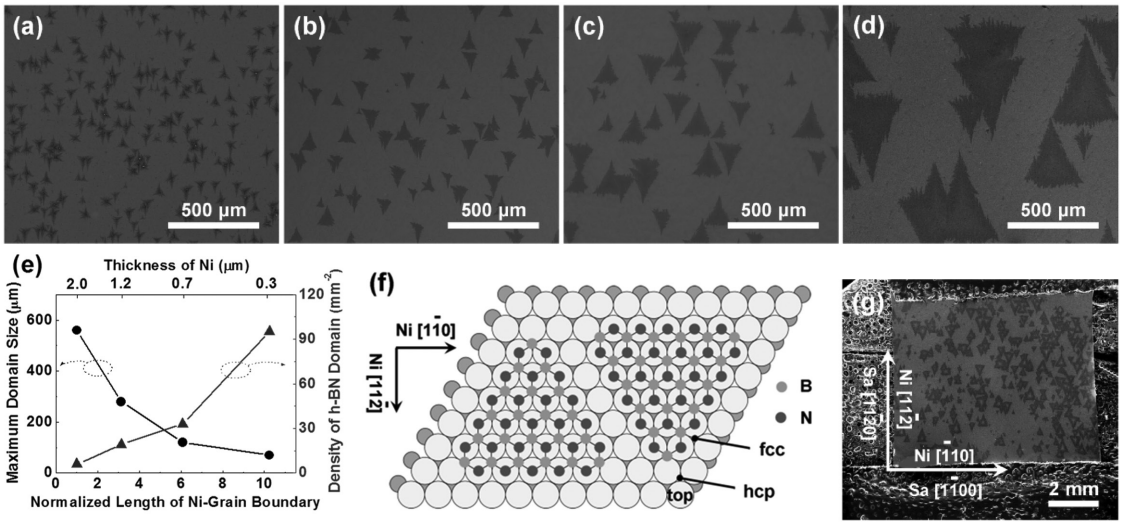

Figure 5. Antiparallel h-BN domains on Ni films with different thicknesses. SEM images of the h-BN domains synthesized on the Ni films with a thickness of a) 0.3, b) 0.7, c) 1.2, and d) 2.0 μm at a fixed growth temperature of 1050 °C and an ion beam density of 0.1 mA cm^{-2} for 15 min. e) The maximum lateral size and the density of h-BN domains as a function of the normalized length of Ni-grain boundaries. f) Structure model of two different orientations of h-BN domains with respect to the underlying Ni (111) substrate. g) Low-magnification SEM image of h-BN domains, showing that the edges of h-BN domains are oriented parallel to the [1$\bar{1}$ 00] direction of sapphire, and thus the [$\bar{1}$ 10] direction of Ni.

the fcc site is preferable, and the hcp configuration is energetically slightly less favorable (9 meV/BN) than the fcc structure.[46] In the present work, the growth of h-BN was performed at high temperatures (≈1000 °C), and the thermal energy is sufficient to exceed the energy difference between the fcc and hcp configurations during the initial nucleation stage. Consequently, both nucleation seeds form, and two antiparallel h-BN domains develop. Furthermore, although there are two in-plane orientations of epitaxial Ni films originated from the *ABC* and *ACB* stacking fault, as revealed by the Φ scans of XRD in Figure S1 (Supporting Information), the resulting h-BN domains are actually equivalent to each other. The low-magnification SEM image (Figure 5g) shows that the edges of h-BN domains are oriented parallel to the [1$\bar{1}$00] direction of sapphire, and thus the [$\bar{1}$10] direction of Ni, further evidencing the epitaxial relationship between h-BN and Ni (111) as shown in Figure 5f.

Although the aligned h-BN domains have been achieved in this work, the two antiparallel h-BN domains with different polarities cannot be seamlessly stitched at the domain boundary. It has been reported that the linear defects are formed at the boundaries between two antiparallel domains, and seamless stitching between aligned h-BN domains can be realized only when the polarities of the domains are the same.[20,22,31,43] It is feasible to obtain a large-size single-crystal h-BN layer with minimal domain boundaries if one could control the orientation of h-BN during nucleation. Reducing the growth temperature is a possible approach to control the initial orientation of h-BN domains relative to the underlying Ni substrate, since a slight energy difference occurs between the fcc and hcp configurations. Moreover, oxygen exposure is another way to control the ratio between two antiparallel domains.[43] However, the factors involved in the origin and control of the initial orientation of h-BN domains are not yet well understood, and additional experiments are needed to achieve single-orientation h-BN domains.

Finally, owing to the thermally stable and chemically inert nature of sapphire, this method allows us for repeated use of sapphire substrates without limit. After the h-BN growth and the following transfer process, the sapphire was cleaned for a second time. **Figure 6**a,b shows the AFM images of the as-cleaned and the repeated sapphire substrates, respectively. The typical step-terrace structure with a step height of 0.43 nm can be obtained for both samples, demonstrating the ultraflat surface of the recycled sapphire substrates. The second cycle h-BN grown on the redeposited Ni/sapphire substrate was characterized by SEM (Figure 6c) and

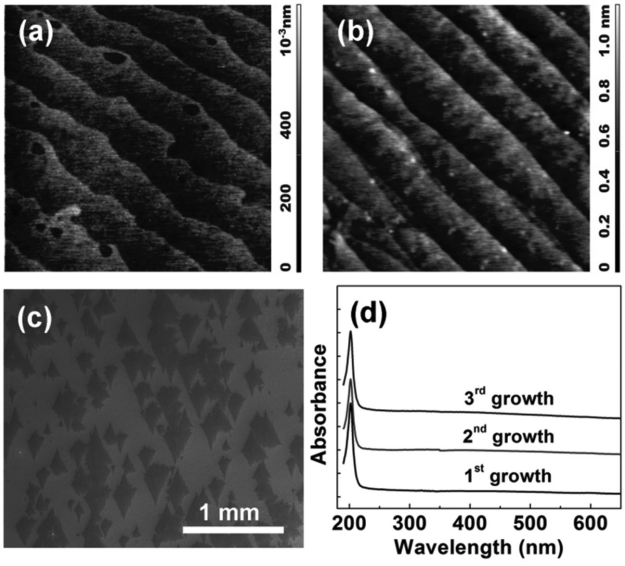

Figure 6. Repeated use of sapphire substrates. AFM images of a) the as-cleaned sapphire and b) the repeated sapphire substrate, showing typical terrace structure with a step height of 0.43 nm. c) SEM image of the h-BN domains grown on the redeposited Ni/sapphire substrate. d) UV–vis spectra of three h-BN films subsequently grown on the same sapphire substrate, showing almost identical features for all the h-BN.

 © 2017 Wiley-VCH Verlag GmbH & Co. KGaA, Weinheim

UV–vis measurements (Figure 6d). The results are highly consistent with the first-grown h-BN, indicating the stability and high quality of the h-BN grown on the repeated sapphire substrate.

3. Conclusions

In summary, we have demonstrated the aligned growth of millimeter-size single-crystal h-BN domains on epitaxial Ni (111)/sapphire substrates by IBSD technique. Under the optimized growth conditions, single-crystal h-BN domains up to 0.6 mm in edge length were obtained. The formation of large-size h-BN domains results mainly from the reduced Ni-grain boundaries and the improved crystallinity of the underlying Ni film. Due to the twinning of the epitaxial Ni (111) film, the h-BN domains show two antiparallel orientations, and the merged h-BN layer exhibits quite uniform and excellent dielectric properties. Our approach to the synthesis of large-size h-BN domains with better alignment represents an important step toward growing the large-area single-crystal h-BN layers for electronic applications.

4. Experimental Section

Heteroepitaxy of Ni Films: The Ni films with various thicknesses were deposited on sapphire (0001) substrates by direct current magnetron sputtering. Prior to deposition, the 0.5 mm thick substrates were dipped into aqueous fluoric acid (10%) for 30 s to remove any residual contaminations and damage. The sputtering chamber was pumped to a base pressure of 2×10^{-5} Pa, then filled with Ar to a working pressure of 1.0 Pa. The Ni films were deposited at 600 °C with a constant sputtering power of 60 W. The deposition time varied from 10 to 90 min, resulting in the thickness of Ni films ranging between 0.3 and 2.5 μm.

Preparation and Transfer of h-BN: The h-BN layers were prepared on the Ni/sapphire substrates in an IBSD chamber equipped with a Kaufmann ion source. The chamber was first evacuated to a base pressure of 2×10^{-5} Pa, and then the Ni/sapphire was annealed at 1050 °C for 20 min under 20 sccm H_2 atmosphere to obtain a clean and smooth surface. Then, the boron and nitrogen species were sputtered from a pure h-BN target by the 1.0 keV Ar ion beam with a constant pressure of 3×10^{-2} Pa at various ion beam densities ranging from 0.1 to 0.4 mA cm^{-2}. During the growth of h-BN, the substrate temperature was held at a constant value ranging from 850 to 1150 °C. After the growth process, the ion source was shut down and the samples were naturally cooled down to room temperature in pure Ar atmosphere. The h-BN was transferred on different substrates for characterization with the same method for graphene. The as-grown samples were spin-coated with poly(methyl methacrylate) (PMMA) on the surface as a supportive layer. After complete etching of the underlying Ni layer, the PMMA/h-BN films were transferred onto the target substrates. Then, PMMA layers were dissolved in acetone leaving the h-BN film for subsequent characterization. The sapphire substrates were cleaned again with the same procedure as the first time for repeated use.

Characterization: The morphology and structure of Ni films and h-BN layers were characterized using SEM (FEI Quanta-450), optical microscope (Olympus BX51M), AFM (NTMDT Solver P47, tapping mode), and TEM (JEOL JEM-2100F, 200 kV). XRD spectra were recorded by Rigaku D/MAX-2500 system using Cu Kα as the X-ray source. Raman spectra were acquired with a Renishaw inVia-Reflex spectrometer using a 532 nm laser as the excitation source. Optical absorption spectra of the samples were measured by a Varian Cary 5000 UV–vis spectrophotometer in a double-beam mode. XPS, NEXAFS, and UPS measurements were carried out for the h-BN on Ni using synchrotron radiation at beam line 4B9B of Beijing Synchrotron Radiation Facility (BSRF). The photon energy is 30 eV for UPS measurements. The tunneling currents through the h-BN layers were measured by conductive AFM using a Solver P47 microscope.

Supporting Information

Supporting Information is available from the Wiley Online Library or from the author.

Acknowledgements

This work was financially supported by the National Natural Science Foundation of China (Nos. 61376007 and 61674137), the National Key Research and Development Program of China (Nos. 2016YFB0400802 and 2016YFB0402301), and the Natural Science Foundation of Beijing Municipality (No. 2142032).

[1] L. Song, L. J. Ci, H. Lu, P. B. Sorokin, C. H. Jin, J. Ni, A. G. Kvashnin, D. G. Kvashnin, J. Lou, B. I. Yakobson, P. M. Ajayan, *Nano Lett.* **2010**, *10*, 3209.
[2] K. K. Kim, A. Hsu, X. T. Jia, S. M. Kim, Y. M. Shi, M. Hofmann, D. Nezich, J. F. Rodriguez-Nieva, M. Dresselhaus, T. Palacios, J. Kong, *Nano Lett.* **2012**, *12*, 161.
[3] M. Xu, T. Liang, M. Shi, H. Chen, *Chem. Rev.* **2013**, *113*, 3766.
[4] J. Yin, J. Li, Y. Hang, J. Yu, G. Tai, X. Li, Z. Zhang, W. Guo, *Small* **2016**, *12*, 2942.
[5] C. R. Dean, A. F. Young, I. Meric, C. Lee, L. Wang, S. Sorgenfrei, K. Watanabe, T. Taniguchi, P. Kim, K. L. Shepard, J. Hone, *Nat. Nanotechnol.* **2010**, *5*, 722.
[6] Z. Liu, L. L. Ma, G. Shi, W. Zhou, Y. J. Gong, S. D. Lei, X. B. Yang, J. N. Zhang, J. J. Yu, K. P. Hackenberg, A. Babakhani, J.-C. Idrobo, R. Vajtai, J. Lou, P. M. Ajayan, *Nat. Nanotechnol.* **2013**, *8*, 119.
[7] A. S. Mayorov, R. V. Gorbachev, S. V. Morozov, L. Britnell, R. Jalil, L. A. Ponomarenko, P. Blake, K. S. Novoselov, K. Watanabe, T. Taniguchi, A. K. Geim, *Nano Lett.* **2011**, *11*, 2396.
[8] K. H. Lee, H.-J. Shin, J. Lee, I.-Y. Lee, G.-H. Kim, J.-Y. Choi, S.-W. Kim, *Nano Lett.* **2012**, *12*, 714.
[9] L. Britnell, R. V. Gorbachev, R. Jalil, B. D. Belle, F. Schedin, A. Mishchenko, T. Georgiou, M. I. Katsnelson, L. Eaves, S. V. Morozov, N. M. R. Peres, J. Leist, A. K. Geim, K. S. Novoselov, L. A. Ponomarenko, *Science* **2012**, *335*, 947.
[10] Y. Wan, H. Zhang, W. Wang, B. W. Sheng, K. Zhang, Y. L. Wang, Q. J. Song, N. N. Mao, Y. P. Li, X. Q. Wang, J. Zhang, L. Dai, *Small* **2016**, *12*, 198.
[11] G.-H. Lee, X. Cui, Y. D. Kim, G. Arefe, X. Zhang, C.-H. Lee, F. Ye, K. Watanabe, T. Taniguchi, P. Kim, J. Hone, *ACS Nano* **2015**, *9*, 7019.

 © 2017 Wiley-VCH Verlag GmbH & Co. KGaA, Weinheim

[12] M. S. Bresnehan, M. J. Hollander, M. Wetherington, M. LaBella, K. A. Trumbull, R. Cavalero, D. W. Snyder, J. A. Robinson, *ACS Nano* **2012**, *6*, 5234.
[13] G. Lu, T. Wu, Q. Yuan, H. Wang, H. Wang, F. Ding, X. Xie, M. Jiang, *Nat. Commun.* **2015**, *6*, 6160.
[14] M. H. Khan, Z. Huang, F. Xiao, G. Casillas, Z. Chen, P. J. Molino, H. K. Liu, *Sci. Rep.* **2015**, *5*, 7743.
[15] Y. Gao, W. Ren, T. Ma, Z. Liu, Y. Zhang, W.-B. Liu, L.-P. Ma, X. Ma, H.-M. Cheng, *ACS Nano* **2013**, *7*, 5199.
[16] C. H. Zhang, L. Fu, S. L. Zhao, Y. Zhou, H. L. Peng, Z. F. Liu, *Adv. Mater.* **2014**, *26*, 1776.
[17] H. L. Wang, X. W. Zhang, J. H. Meng, Z. G. Yin, X. Liu, Y. J. Zhao, L. Q. Zhang, *Small* **2015**, *11*, 1542.
[18] L. F. Wang, B. Wu, J. S. Chen, H. T. Liu, P. A. Hu, Y. Q. Liu, *Adv. Mater.* **2014**, *26*, 1559.
[19] R. Y. Tay, M. H. Griep, G. Mallick, S. H. Tsang, R. S. Singh, T. Tumlin, E. H. T. Teo, S. P. Karna, *Nano Lett.* **2014**, *14*, 839.
[20] C. M. Orofeo, S. Suzuki, H. Kageshima, H. Hibino, *Nano Res.* **2013**, *6*, 335.
[21] X. J. Song, J. F. Gao, Y. F. Nie, T. Gao, J. Y. Sun, D. L. Ma, Q. C. Li, Y. B. Chen, C. H. Jin, A. Bachmatiuk, M. H. Rümmeli, F. Ding, Y. F. Zhang, Z. F. Liu, *Nano Res.* **2015**, *8*, 3164.
[22] Q. Wu, J.-H. Park, S. Park, S. J. Jung, H. Suh, N. Park, W. Wongwiriyapan, S. Lee, Y. H. Lee, Y. J. Song, *Sci. Rep.* **2015**, *5*, 16159.
[23] Y. Stehle, H. M. Meyer III, R. R. Unocic, M. Kidder, G. Polizos, P. G. Datskos, R. Jackson, S. N. Smirnov, I. V. Vlassiouk, *Chem. Mater.* **2015**, *27*, 8041.
[24] S. Caneva, R. S. Weatherup, B. C. Bayer, B. Brennan, S. J. Spencer, K. Mingard, A. Cabrero-Vilatela, C. Baehtz, A. J. Pollard, S. Hofmann, *Nano Lett.* **2015**, *15*, 1867.
[25] H. L. Wang, X. W. Zhang, H. Liu, Z. G. Yin, J. H. Meng, J. Xia, X.-M. Meng, J. L. Wu, J. B. You, *Adv. Mater.* **2015**, *27*, 8109.
[26] A. Goriachko, Y. He, M. Knapp, H. Over, M. Corso, T. Brugger, S. Berner, J. Osterwalder, T. Greber, *Langmuir* **2007**, *23*, 2928.
[27] P. Sutter, J. Lahiri, P. Zahl, B. Wang, E. Sutter, *Nano Lett.* **2013**, *13*, 276.
[28] F. Orlando, P. Lacovig, L. Omiciuolo, N. G. Apostol, R. Larciprete, A. Baraldi, S. Lizzit, *ACS Nano* **2014**, *8*, 12063.
[29] A. Nagashima, N. Tejima, Y. Gamou, T. Kawai, C. Oshima, *Phys. Rev. B* **1995**, *51*, 4606.
[30] J. Yin, X. F. Liu, W. L. Lu, J. D. Li, Y. Z. Cao, Y. Li, Y. Xu, X. M. Li, J. Zhou, C. H. Jin, W. L. Guo, *Small* **2015**, *11*, 5375.
[31] R. Y. Tay, H. J. Park, G. H. Ryu, D. Tan, S. H. Tsang, H. Li, W. W. Liu, E. H. T. Teo, Z. Lee, Y. Lifshitzg, R. S. Ruoff, *Nanoscale* **2016**, *8*, 2434.
[32] H. Bialas, K. Heneka, *Vacuum* **1994**, *45*, 79.
[33] V. I. Artyukhov, Y. Hao, R. S. Ruoff, B. I. Yakobson, *Phys. Rev. Lett.* **2015**, *114*, 115502.
[34] R. Geick, C. H. Perry, G. Rupprecht, *Phys. Rev.* **1966**, *146*, 543.
[35] A. B. Preobrajenski, A. S. Vinogradov, N. Mårtensson, *Surf. Sci.* **2005**, *582*, 21.
[36] A. A. Tonkikh, E. N. Voloshina, P. Werner, H. Blumtritt, B. Senkovskiy, G. Güntherodt, S. S. P. Parkin, Yu S. Dedkov, *Sci. Rep.* **2016**, *6*, 23547.
[37] W. Auwärter, T. J. Kreutz, T. Greber, J. Osterwalder, *Surf. Sci.* **1999**, *429*, 229.
[38] J. Tauc, *Mater. Res. Bull.* **1968**, *3*, 37.
[39] G. Cassabois, P. Valvin, B. Gil, *Nat. Photonics* **2016**, *10*, 262.
[40] K. Watanabe, T. Taniguchi, H. Kanda, *Nat. Mater.* **2004**, *3*, 404.
[41] T. Greber, W. Auwärter, M. Hoesch, G. Grad, P. Blaha, J. Osterwalder, *Surf. Rev. Lett.* **2002**, *9*, 1243.
[42] G.-H. Lee, Y.-J. Yu, C. Lee, C. Dean, K. L. Shepard, P. Kim, J. Hone, *Appl. Phys. Lett.* **2011**, *99*, 243114.
[43] W. Auwärter, M. Muntwiler, J. Osterwalder, T. Greber, *Surf. Sci.* **2003**, *545*, L735.
[44] W. Auwärter, H. U. Suter, H. Sachdev, T. Greber, *Chem. Mater.* **2004**, *16*, 343.
[45] Y. Liu, S. Bhowmick, B. I. Yakobson, *Nano Lett.* **2011**, *11*, 3113.
[46] G. B. Grad, P. Blaha, K. Schwarz, W. Auwärter, T. Greber, *Phys. Rev. B* **2003**, *68*, 085404.

Received: December 17, 2016
Revised: January 9, 2017
Published online:

 © 2017 Wiley-VCH Verlag GmbH & Co. KGaA, Weinheim